

Role of Low Clouds in Summertime Atmosphere–Ocean Interactions over the North Pacific

JOEL R. NORRIS,* YUAN ZHANG, AND JOHN M. WALLACE

Department of Atmospheric Sciences, University of Washington, Seattle, Washington

(Manuscript received 14 July 1997, in final form 1 December 1997)

ABSTRACT

The summer-to-summer variability of the areal extent of marine stratiform cloudiness (MSC; stratus, stratocumulus, and fog) over the North Pacific is examined for the period of record 1952–92 using a dataset based on surface observations. Variability is largest in two regions: the central and western Pacific along 35°N coincident with a strong meridional gradient in climatological MSC amount, and the eastern Pacific near 15°N downstream of the persistent stratocumulus deck off Baja California. The MSC amount in both regions tends to be negatively correlated with local sea surface temperature (SST), suggestive of a positive cloud feedback on SST. The MSC amounts in the two regions also tend to be negatively correlated by virtue of their relationship to the basin-wide sea level pressure (SLP) field: a strengthening of the seasonal mean subtropical anticyclone is accompanied by increased cloudiness in the trade wind regime and decreased cloudiness in the southerly flow farther toward the west. These relationships are reflected in the leading modes derived from empirical orthogonal function analysis and singular value decomposition analysis of the MSC, SST, and SLP fields.

From the 1950s to the 1980s, summertime MSC amounts increased in the central and western Pacific and decreased in the trade wind region, while SST exhibited the opposite tendencies. Although these trends contributed to the relationships described above, similar patterns are obtained when the analysis is performed on 1-yr difference fields (e.g., 1953 minus 1952, 1954 minus 1953, etc.). Hence, it appears that MSC plays an important role in atmosphere–ocean coupling over the North Pacific during the summer season when latent and sensible heat fluxes are not as dominant and the coupling between atmospheric circulation and SST is not as strong as in winter.

1. Introduction

In the companion paper, Zhang et al. (1998, hereafter referred to as ZNW) showed that the dominant mode of interannual SST variability over the North Pacific can be viewed as a year-round pattern that exhibits only minor seasonal variations. Along 40°N to the west of 150°W, and in the subtropical eastern Pacific, SST anomalies tend to persist year round. The season-to-season persistence of the basin-wide SST pattern is much stronger than that of local SST anomalies. Based on simple models of the ocean mixed layer, as reviewed by Frankignoul (1985), this year-round persistence is difficult to reconcile with the shallowness of the summertime mixed layer. It would seem that some sort of positive feedback is needed in order to sustain the anomalies through the summer season, when the atmospheric

Pacific–North American (PNA) pattern is largely absent and the linkages between the anomalous SST and geopotential height fields are relatively weak, as illustrated in Table 1.

Norris and Leovy (1994) have suggested that interactions between low, stratiform cloud decks [hereafter referred to as “marine stratiform cloudiness” (MSC)] and SST might contribute to the persistence of midlatitude SST anomalies. Because of its large areal extent, MSC exerts a strong influence on the energy balance at the top of the atmospheric planetary boundary layer and (through the convective adjustment process) at the air–sea interface as well. Assuming a cloud albedo of 35%, each 1% increase in cloud cover reduces by 1 W m^{-2} the energy available for heating the ocean: enough to cool a 25-m-deep mixed layer by $\sim 0.1 \text{ K}$ over the course of a summer season. The SST, in turn, has the potential to influence the fractional coverage of certain types of boundary layer cloud decks that may be highly sensitive to the ambient static stability. Klein and Hartmann (1993) examined the relationship between the MSC amount and the surface to 700-mb potential temperature difference based on climatological mean data for different parts of the world ocean in different seasons. Their regression analysis indicates that if the 700-mb

* Current affiliation: National Center for Atmospheric Research, Boulder, Colorado.

Corresponding author address: Joel Norris, Advanced Studies Program, National Center for Atmospheric Research, P.O. 3000, Boulder, CO 80307-3000.
E-mail: jnorris@ucar.edu

TABLE 1. Summary statistics for the leading singular value decomposition mode for the seasonal mean North Pacific SST field paired with the hemispheric 500-mb height field, both poleward of 18°N. For details of the calculation, see section 2 of the companion paper Zhang et al. (1998). Here SCF is squared covariance fraction, NC is normalized root-mean-square, and r is correlation of expansion coefficient time series.

	SCF	NC	r
Winter	68	20	84
Summer	37	10	63

temperature remained constant, a decrease in surface air temperature of 0.2 K would result in a 1% increase in the MSC amount: enough to constitute a strong positive feedback, locally.

If such a feedback is operative over the North Pacific, the SST and MSC amount should be negatively correlated at fixed grid points. Norris and Leovy (1994) have demonstrated the existence of such a negative correlation with values in excess of 0.5 in the vicinity of the primary center of action of the leading EOF of the SST field during summertime. It remains to be demonstrated that spatial patterns of SST and cloudiness are related in such a way as to suggest the existence of a positive feedback during summer. To this end, we will document the temporal standard deviation and leading EOF of MSC amount over the North Pacific during summertime and relate the dominant patterns in MSC, SST, and sea level pressure using singular value decomposition (SVD) analysis, as detailed in the companion paper.

2. Data

The MSC dataset used in this paper covers the period 1952–92 and was obtained by averaging individual surface observations of stratocumulus, stratus, and sky-obscuring fog from an updated version of the Edited Cloud Report Archive (Hahn et al. 1996) to form seasonal means on the same 10° latitude × 20° longitude grid used by Warren et al. (1988).¹ Although we use the same original raw data and “stratus” cloud category as did Warren et al., our MSC dataset differs from theirs in that it does not suffer from biases due to changes in spatial and diurnal sampling. Means over such large grid boxes are highly sensitive to spatial sampling, which has varied from year-to-year and from decade-to-decade. For example, boxes along 40°N in the central Pacific exhibit a spurious upward trend in cloudiness due to a slight northward shift in the major trans-Pacific shipping routes from the 1950s to the 1980s. In order to reduce this sensitivity, MSC was first averaged over

2.5° lat × 5° long boxes and these averages were aggregated into the larger boxes without weighting by number of observations. Changes in the relative fraction of day/night observations can also produce a bias in regions where MSC amount exhibits a large diurnal cycle. Because observers sometimes have difficulty identifying cloudiness under conditions of poor illumination (Hahn et al. 1995; Rozendaal et al. 1995) we elected to use only daytime (including twilight) observations.

In recognition of the susceptibility of the MSC data to other spurious long-term trends arising from subtle changes in observing practices that may have occurred over the years (e.g., Bajuk and Leovy 1998), the variance, EOF, and SVD calculations shown in the next section were all repeated on 1-yr (summer-to-summer) difference fields, which emphasize the high-frequency variability in the record. With few exceptions, the results based on the unfiltered data described in the next section proved to be reproducible. A brief summary of the results based on difference fields is presented in section 4.

The SST and sea level pressure (SLP) data are from the Comprehensive Ocean–Atmosphere DataSet (COADS). They are aggregated in 4° lat × 6° long grid boxes as described in ZNW. The SST data are for the same period of record (1952–92) as the cloud data and the SLP record ends a year earlier. All calculations are based on the full 41-yr record except those involving SLP, which are for a 40-yr record.

3. Results based on unfiltered fields

For reference, the climatological mean distribution of MSC amount for summer (June, July, and August) is shown in Fig. 1 in the standard 10° lat × 20° long format and (for this figure only) in a 2.5° lat × 5° long format. The higher-resolution version resembles the distribution of net cloud radiative forcing derived from the Earth Radiation Budget Experiment (Harrison et al. 1990). Poleward of 35°N the fractional sky cover is generally in excess of 40%, with values ranging up to 80% over the Bering Sea during summer. The contours dip southward to encompass the persistent stratocumulus deck off the coast of California, which shows up as a separate (60%+) maximum in the high-resolution version. In these regions, cloud cover is more extensive during summer than during winter. Across most of the Pacific, summertime MSC amount exhibits a strong meridional gradient between 30°N and 45°N with values on the order of 5% per degree of latitude. As pointed out by Klein and Hartmann (1993), the cloudiness contours in this region tend to follow the SST isotherms, with more extensive cloudiness over the colder waters to the north where the lower tropospheric static stability is higher. Equatorward of 35°N cumulus cloud types dominate, whereas poleward of that latitude stratiform cloud types dominate (Warren et al. 1988).

The standard deviation of summertime MSC amount, shown in Fig. 2, exhibits a considerable amount of struc-

¹ As in Warren et al., the longitudinal extent of the boxes is slightly greater poleward of 50° in order to make them roughly comparable in area to the lower latitude boxes.

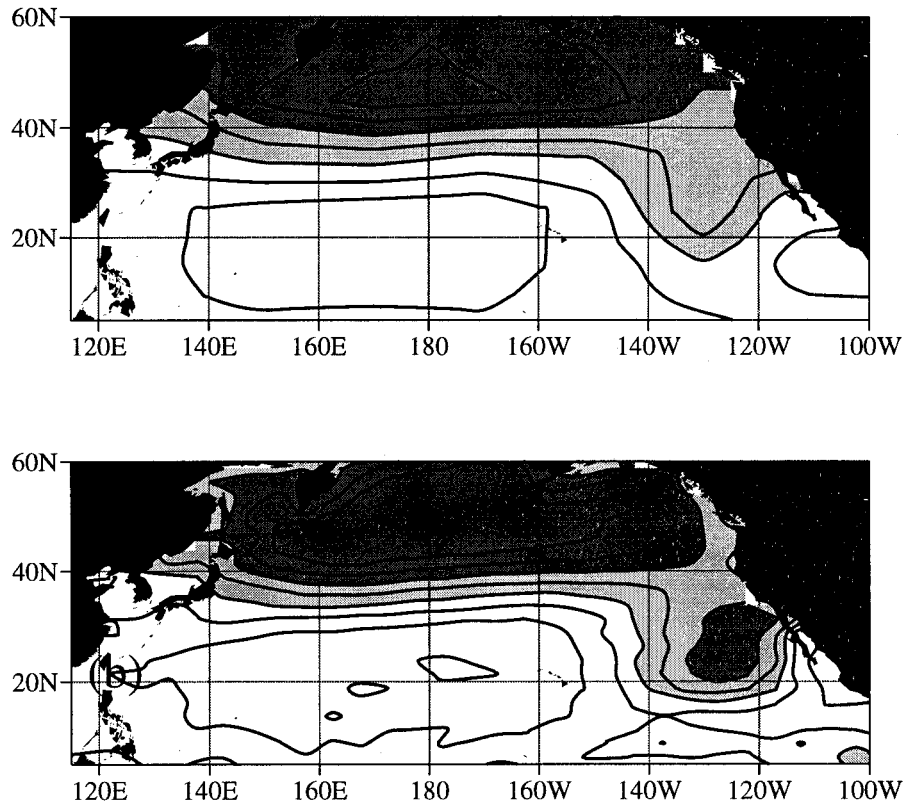


FIG. 1. Climatological mean sky coverage by marine stratiform cloudiness (MSC) based on the period of record 1952–92: (top) 10° lat \times 20° long resolution and (bottom) 2.5° lat \times 5° long resolution. Contour interval 10%: thresholds for lighter (darker) shading are 40% (60%).

ture, with maxima along the Asian and California coasts, in a band along 35°N in the western and central Pacific coinciding with the strong meridional gradient of climatological-mean MSC amount, and along the southern flank of the persistent stratocumulus deck to the west of Baja California. The two regions of high variability remote from the coastline occur in contrasting climatic regimes: the former corresponds to a region of mean southerly surface winds and warm advection, and the

latter to a region of northeasterly trade winds and cold advection.

Figure 3 shows the leading EOF of summertime MSC amount that accounts for 20% of variance over the entire North Pacific from poleward of 10°N . Its two centers of action, of opposing polarity, correspond to the variance maxima (remote from the coast) in the previous figure. Evidently, when summertime cloudiness is above normal along 35°N in the central and western Pacific,

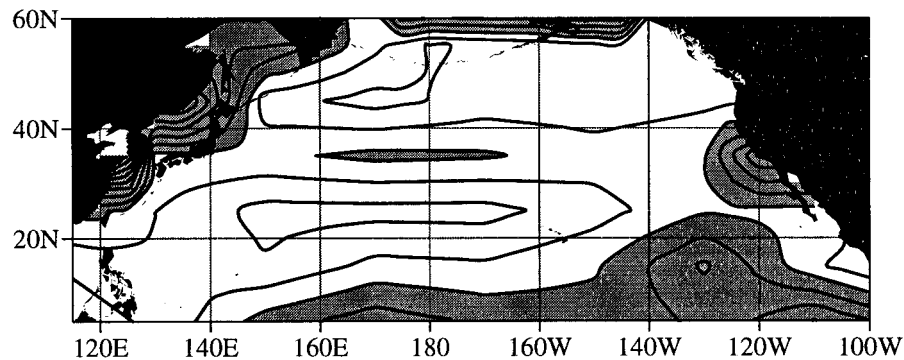


FIG. 2. Standard deviations of summertime-mean MSC. Contour interval 1%: the threshold for shading is 5%.

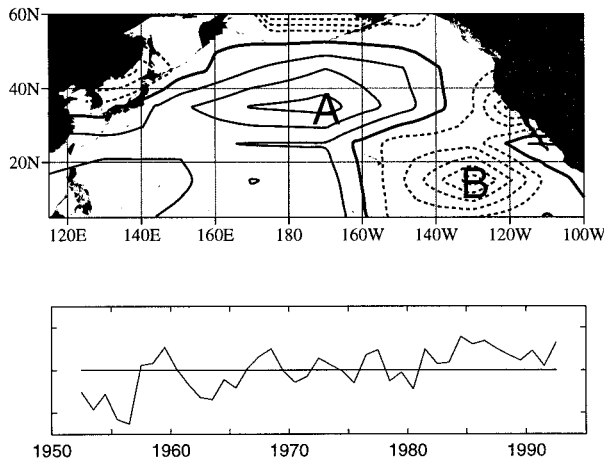


FIG. 3. Leading EOF of the summertime MSC field based on seasonal-mean data, scaled as described in section 2 of ZWN. Contour interval 1%: the zero contour is thickened and negative contours are dashed. The lower panel shows the corresponding normalized PC time series: one tick mark represents two standard deviations.

it tends to be below normal to the west of Baja California and vice versa. That this inverse relation is not an artifact of the EOF analysis is evidenced by the negative correlation (-0.43) between the time series representing summertime MSC anomalies near the two opposing centers of action: area averages A (30° – 40° N, 160° W– 180°) and B (10° – 20° N, 140° – 120° W). Furthermore, center of action A shows up clearly in the one-point correlation map for B and vice versa (not shown).

The corresponding PC time series shown in the lower panel of the figure exhibits a marked upward trend from the 1950s to the 1980s, with a rise of about two standard deviations. During this period, the mean summertime MSC amount increased from 35% to 40% in region A and decreased from 41% to 33% in region B, in qualitative agreement with the trends computed by Warren et al. (1988).² We will consider the extent to which the structure of the EOF is a reflection of these trends in the next section.

To investigate the relationships between the summertime MSC, SST, and SLP fields, SVD analysis was performed upon all three pairs of variables for the North Pacific domain, poleward of 18° N for SST and SLP and poleward of 10° N for MSC. The summary statistics, shown schematically in Fig. 4, indicate that the MSC amount is strongly coupled to both SST and SLP, whereas SST and SLP are only relatively weakly coupled. The leading singular vectors for the three expansions are shown in Figs. 5 (MSC/SST), 6 (MSC/SLP), and 7 (SST/SLP). For reference, the leading EOF of summertime SLP in the same domain is shown in Fig. 8,

² The trends computed by Warren et al. were substantially larger, presumably because of the changes in spatial sampling discussed in section 2.

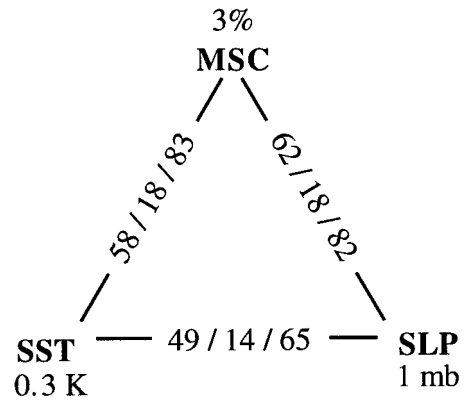


FIG. 4. Summary statistics for the SVD analyses, with the MSC, SST, and SLP fields paired as indicated. The format is SCF/NC/ r , all expressed in percent. The numbers at the vertices of the triangles represent typical amplitudes of the coupled perturbations at the primary centers of action of the respective patterns. Here SCF is squared covariance fraction, NC is normalized root-mean-square, and r is correlation of expansion coefficient time series.

together with its PC time series. In all four figures the values plotted on the maps are in dimensional units and represent typical amplitudes of the patterns. They were derived by regressing the various fields upon the time series of the respective normalized expansion coefficients. Amplitudes at the major centers of action are included in the summary statistics presented in Fig. 4.

The patterns for MSC/SST in Fig. 5 resemble their respective EOFs in Figs. 3 of this paper and 4 of ZNW, and the patterns for MSC/SLP in Fig. 6 resemble their respective EOFs in Figs. 3 and 8. The temporal behavior of the SVD expansion coefficients (not shown) can be

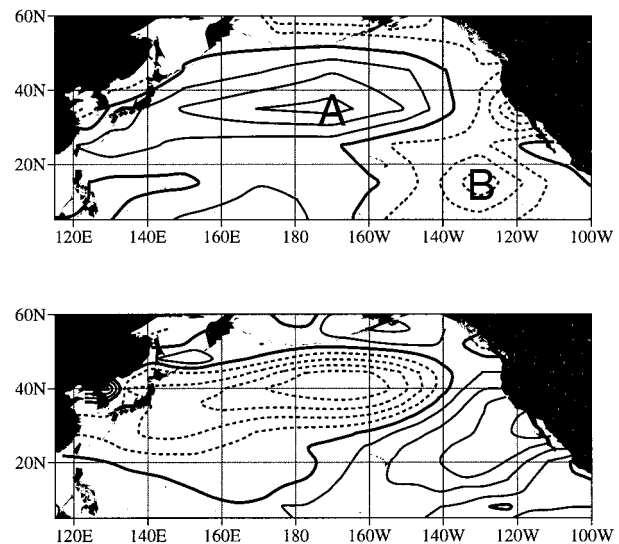


FIG. 5. Leading SVD mode for (top) MSC paired with (bottom) SST in summer. Contour intervals 1% and 0.1 K: the zero contour is thickened and negative contours are dashed. Summary statistics are presented in Fig. 4.

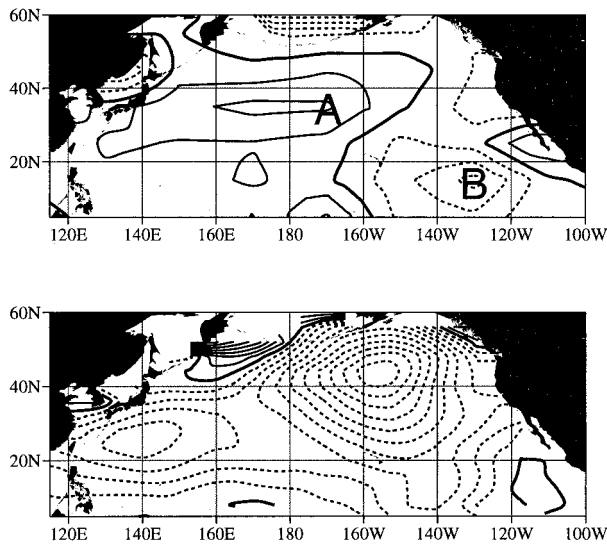


FIG. 6. Leading SVD mode for (top) MSC paired with (bottom) SLP in summer. Contour intervals 1% and 0.1 mb; the zero contour is thickened and negative contours are dashed. Summary statistics are presented in Fig. 4.

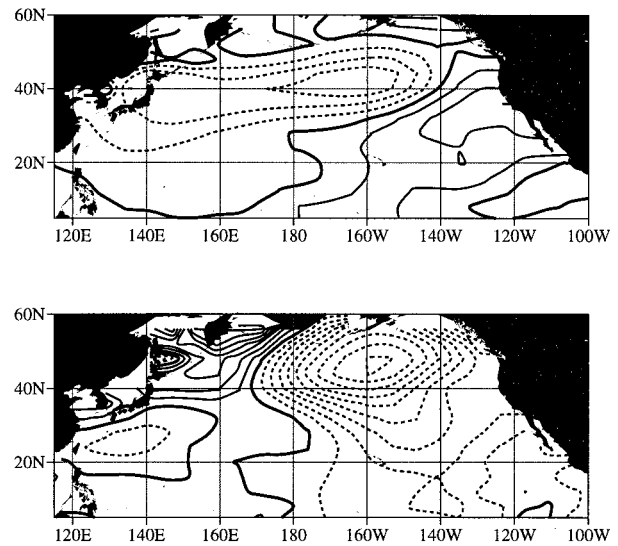


FIG. 7. Leading SVD mode for (top) SST paired with (bottom) SLP in summer. Contour intervals 0.1 K and 0.1 mb; the zero contour is thickened and negative contours are dashed. Summary statistics are presented in Fig. 4.

inferred from the PC time series that accompany the corresponding EOFs.

In agreement with results of Norris and Leovy (1994), above normal MSC amount occurs in association with below normal SST at both major centers of action. It can be inferred from the corresponding SLP pattern (Fig. 6) that in region B west of Baja California, positive MSC anomalies occur in association with anomalous northeasterly winds and enhanced cold advection, consistent with results of Klein et al. (1995) based on data for Ocean Weather Ship N (30°N, 140°W). In region A in the central Pacific the relationship between the MSC amount and surface wind anomalies is less clear. The SLP pattern in Fig. 6 can be recovered by regressing the SLP field upon MSC time series near centers of action A and B (not shown). Similar spatial patterns emerge when SLP is paired directly with SST (Fig. 7) without using MSC as an intermediary, but the relationships are not as strong. Negative SST anomalies along 40°N occur in association with anomalously weak southerly winds westward of 160°W, and positive SST anomalies west of Baja California occur in association with anomalously weak trade winds.

The standardized amplitudes of the MSC, SST, and SLP anomalies in Fig. 4 are rough estimates derived from inspection of Figs. 5–7 and are representative of conditions in the vicinity of the major centers of action of the respective fields. The SST anomalies appear to be roughly comparable in amplitude to those associated with the leading mode of wintertime coupled atmosphere–ocean variability, but the SLP anomalies, as inferred from the SVD analysis, are weaker, by a factor of 5, than those observed during wintertime. Furthermore, SLP is less strongly coupled to SST during sum-

mer time than during wintertime, when the atmospheric PNA pattern is involved. In contrast, the MSC anomalies tend to be stronger and much more strongly coupled to the other fields during summertime than during wintertime (not shown).

4. Results based on difference fields

The leading principal component (PC) of MSC amount (Fig. 4) exhibits a conspicuous trend that accounts for almost half the variance. The existence of a corresponding trend in the leading PC of SST (ZNW

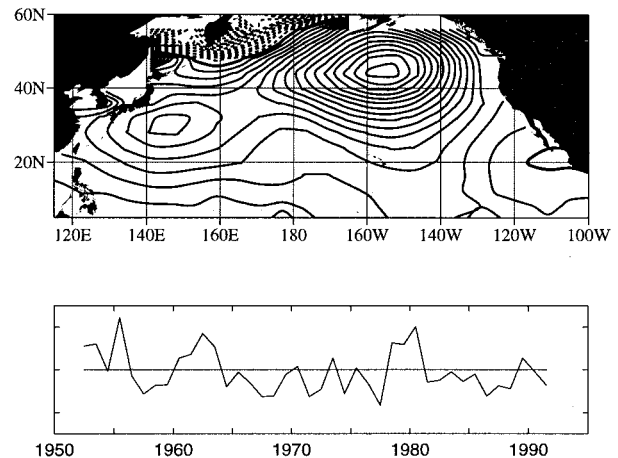


FIG. 8. Leading EOF of the summertime SLP field based on seasonal-mean data, scaled as described in section 2 of ZWN. Contour interval 0.1 mb; the zero contour is thickened and negative contours are dashed. The lower panel shows the corresponding normalized PC time series. One tick mark represents two standard deviations.

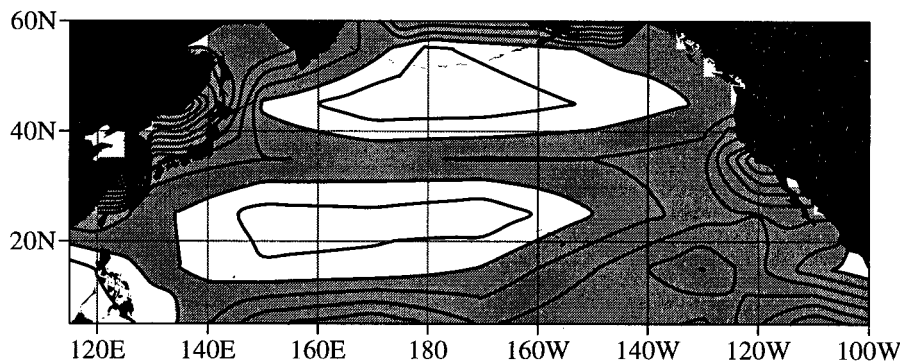


FIG. 9. Standard deviation of MSC differences from one summer to the next. Contour interval 0.5%: the threshold for shading is 2.5%.

Fig. 4) lends credence to this feature. However, in view of the sensitivity of the MSC data to factors such as subtle biases in reporting practices, one might question whether some of the large trend in the MSC data might be spurious. Even if it were real, one might question whether, in the presence of such trends, the MSC field possesses enough temporal degrees of freedom to ensure that the results presented in the previous section would be reproducible in an independent dataset. To address these questions we repeated the analysis using 1-yr differences of MSC amount and SST in place of the values themselves (e.g., replacing the 1953 values with those for 1953 minus 1952, etc.). This one-step time differencing acts as a strong high-pass filter, accentuating variability with periods ranging from 2 yr out to ~5 yr and virtually eliminating any interdecadal trends in the data.

The standard deviation field, shown in Fig. 9, strongly resembles its unfiltered counterpart in Fig. 2. The leading EOF (Fig. 10), which accounts for 15% of the variance, also resembles its counterpart for the MSC field itself (Fig. 3), but center of action off Baja California is more prominent than the one in the central Pacific. In general, long-range teleconnections in the MSC difference field tend to be weaker and less robust than those in the MSC field itself. In recognition of this more local character of the summer-to-summer differences in MSC amount, we show here, in place of the SVD results in

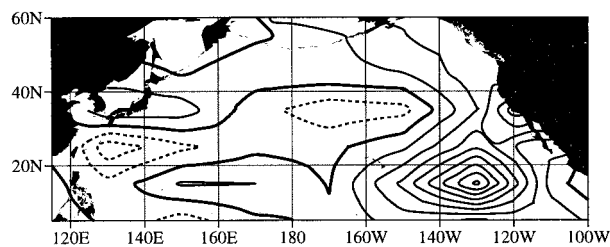


FIG. 10. Leading EOF of the MSC difference field based on seasonal-mean data, scaled as described in section 2 of ZWN. Contour interval 1%: the zero contour is thickened and negative contours are dashed.

the previous section, a series of one-point regression maps based on MSC differences at three representative gridpoints: A and B as defined in the previous section, and C (30°–40°N, 120°–140°W).

The regression maps for the SST field, shown in Fig. 11, confirm the existence of strong negative local correlations between MSC amount and SST. Absolute values (not shown) range as high as 0.77 for point A, 0.69

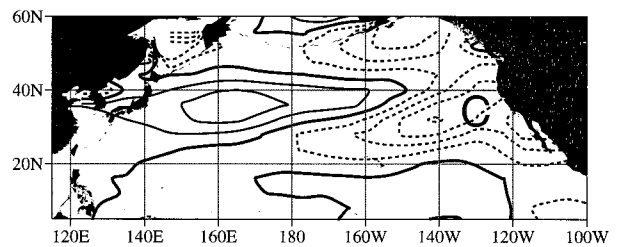
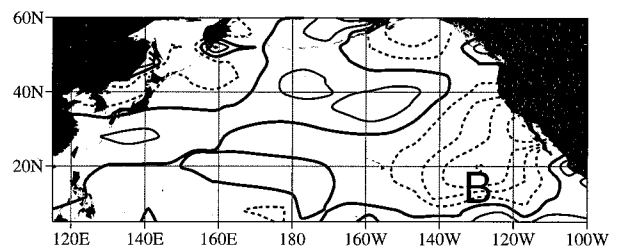
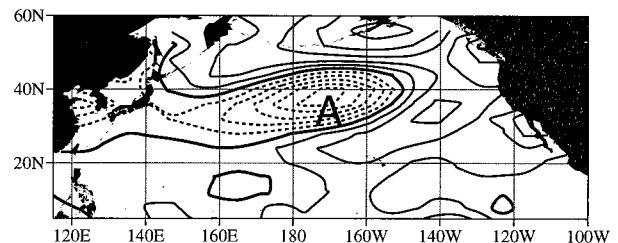


FIG. 11. SST difference field regressed upon the normalized MSC difference time series for grid boxes A, B, and C, as indicated. Contour interval 0.1 K: the zero contour is thickened and negative contours are dashed.

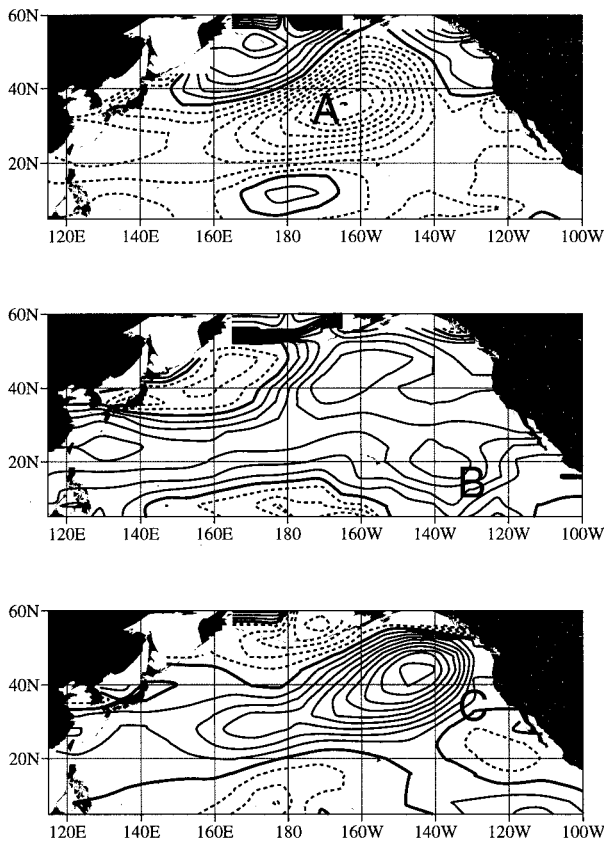


FIG. 12. SLP difference field regressed upon the normalized MSC difference time series for grid boxes A, B, and C, as indicated. Contour interval 0.1 mb; the zero contour is thickened and negative contours are dashed.

for B, and 0.68 for C. The corresponding regression coefficients are on the order of 0.1 K per percent change in MSC amount near point A, 0.05 K at B, and 0.07 K at C. The corresponding regression maps for the SLP field are shown in Fig. 12. The pattern for point A resembles the leading EOF of the summertime SLP field (Fig. 8) and the leading EOF of the SLP difference field (not shown) that its primary center of action coincides with the climatological-mean subtropical anticyclone. A strengthening of the anticyclone favors reduced cloudiness at A and vice versa: a 1% decrease in the MSC amount occurs in association with an increase in the central pressure of the anticyclone of ~ 0.2 mb. Summer-to-summer differences in MSC amount at B are evidently associated with changes in the strength of the trade winds in the vicinity of the reference grid point, consistent with results of Klein et al. (1995) based on data for Ocean Weather Ship N (30°N , 140°W). Based on geostrophic winds inferred from the SLP regressions, a 1% increase in the MSC amount is observed in association with a ~ 0.1 m s^{-1} increase in the strength of the trade winds at both points B and C, again consistent with results of Klein et al.

These results serve to confirm the existence of strong

coupling between summertime MSC amount and the SST and SLP fields over the North Pacific, irrespective of whatever spurious trends might be present in the MSC data.

5. Discussion

The observational evidence presented in the previous section supports the notion that large-scale atmosphere-ocean interaction during summertime and wintertime might be fundamentally different in character. SST anomalies are of comparable magnitude during the two seasons, but the SLP and surface wind anomalies associated with the leading mode of coupled variability are much stronger during winter, giving rise to strong latent and sensible heat fluxes that dominate the surface energy budget and the generation of SST anomalies. On the other hand, MSC exhibits more coherent, large-scale organization and is more strongly coupled to the dominant SST pattern during summer, which, together with the greater insolation, favors a stronger influence of radiative fluxes upon the evolution of SST anomalies. The prevalence of negative correlations between MSC and SST anomalies in the leading coupled mode of summer-to-summer variability supports the notion that a positive feedback might be operative in which enhanced cloudiness cools the mixed layer and lower SST favors enhanced cloudiness by modifying the structure of the atmospheric boundary layer. A simple analysis conducted within the framework of the passive ocean mixed layer formalism of Hasselmann (1976) and Frankignoul (1985) indicates that such a feedback could substantially lengthen the persistence time of summertime SST anomalies (Zhang 1996). The strong similarity between the patterns of MSC amount and SST in the leading SVD mode and leading EOFs of the MSC and SST fields suggests that the dominant mode of SST variability, with its strong memory from one season to the next, might be instrumental in shaping the variability of summertime-mean MSC anomalies.

Summer-to-summer variability in MSC amount also appears to be strongly coupled to relatively weak fluctuations in SLP that its spatial structure closely resembles the leading EOF of that field. To first order, the amplitude of this pattern can be characterized as a measure of the strength of the broad anticyclone that dominates the low-level summertime flow over much of the North Pacific. A strengthening of the anticyclone is attended by increased cloudiness in the trade wind region of the eastern Pacific and reduced cloudiness along 35°N in the central and western Pacific. The former can be understood as resulting from enhanced cold advection and possibly enhanced subsidence, which favor a moister and shallower boundary layer, thus producing a downstream displacement of the transition from stratocumulus to trade cumulus regimes (Klein et al. 1995). The latter can be understood as resulting from the poleward

retreat of the mean summertime storm track and its attendant stratiform cloudiness.

The fact that the central North Pacific centers of action in the MSC/SST SVD analysis (Fig. 5) are located at the sharp transition zone between the colder and more cloudy stratiform regime to the north and the warmer and less cloudy cumuliform regime to the south suggests that MSC/SST variability results from latitudinal shifts of this transition zone. It is evident from Fig. 1 that a poleward displacement of just 1° latitude would be sufficient to account for a 5% decrease in cloud amount. The following mechanisms are proposed to explain the close link between SST and MSC gradients. Equatorward advection of midlatitude stratocumulus over increasingly warm water promotes the breakup of stratocumulus into cumulus, and a displacement of the SST isotherms will produce a corresponding shift of the breakup point. In a similar manner, poleward advection of subtropical cumulus over increasingly cold water promotes a transition from cumulus to stratus, and a displacement of the isotherms will produce a corresponding shift of the transition point. Thus, the transition between stratiform and cumuliform cloudiness follows the SST gradient irrespective of whether the advection is poleward or equatorward.

The above interpretation is consistent with the inverse relationship between MSC amount and lower tropospheric static stability documented by Klein and Hartmann (1993), since a latitudinal shift in the SST gradient will act to produce a corresponding shift in the gradient of static stability. Of course, it is important to keep in mind that variations in the temperature above the marine boundary layer can produce variations in static stability and MSC amount independently of SST. In order to determine the relative contributions of SST variability and free atmosphere temperature variability in modulating MSC, it will be necessary to consider data on temperatures aloft.

Whether the SST and MSC anomalies are capable of feeding back upon the SLP field is not clear from this analysis. The observed SLP anomalies are of the wrong polarity to be interpreted as a linear response to heating resulting from SST anomalies along 40°N , and they do not resemble the pattern that would be expected if they were simply a reflection to the baroclinity in the planetary boundary layer induced by the underlying SST anomalies, as in the formalism of Lindzen and Nigam (1987). The leading coupled SST/SLP patterns are qualitatively similar to their wintertime counterparts, with SLP anomalies situated slightly to the east of SST anomalies of like polarity. Hence, it is conceivable that the SST anomalies feed back barotropically upon the SLP field as they apparently do in winter. On the other hand, the relative weakness of the summertime SLP anomalies raises questions as to whether the associated surface wind anomalies are strong enough to play an essential role in the coupling between the atmosphere and ocean.

Positive cloud feedback could contribute to the re-

markable season-to-season persistence of the leading EOF of SST despite the reemergence of subsurface anomalies each winter season, as documented in the companion paper. However, it is difficult to imagine how positive feedbacks alone could account for the interdecadal variability in SST and summertime MSC (e.g., the drop in SST and the increase in MSC in the central and western Pacific along 35°N from the 1950s to the 1980s). The interdecadal component of the variability would be easier to rationalize if a more conservative variable like salinity were implicated.³

The reemergence mechanism notwithstanding, it may be overly simplistic to treat the coupled climate variability over the North Pacific as if it were inherently a wintertime phenomenon, with subsurface ocean temperature anomalies providing the exclusive source of memory from one winter to the next. The coupling during summer may be important, not only with respect to the memory, but also the evolution of the coupled system from one year to the next. It could conceivably play a role in explaining the distinctive pattern of interdecadal scale climate variability over the North Pacific described by Nitta and Yamada (1989), Trenberth (1990), Trenberth and Hurrell (1994), Graham (1994), Minobe (1997), Zhang et al. (1997), and Mantua et al. (1997).

The questions raised by this exploratory analysis cannot be answered without a more comprehensive investigation involving a quantitative evaluation of the fluxes at the air-sea interface and a more detailed treatment of the cloudiness variability, with separation by specific cloud type. In order to establish causal linkages, it will be necessary to determine whether atmospheric models forced with prescribed SST anomalies are capable of simulating the observed summer-to-summer variability of MSC amount, and conversely, whether ocean models forced with prescribed seasonal and year-to-year variations in insolation are capable of simulating the observed space-time variability of SST. It will be of interest to determine whether coupled models are capable of simulating the coupled interactions described in this paper, and if so, whether they can provide further insights as to how they arise.

Acknowledgments. This work was supported by the National Science Foundation through the Climate Dynamics Program under Grant ATM 9215512 and by NASA through the Earth Observing System Program under Grant NAGW-2633.

REFERENCES

- Frankignoul, C., 1985: Sea surface temperature anomalies, planetary waves and air-sea feedback in the middle latitudes. *Rev. Geophys.*, **23**, 357–390.

³ A suggestion by P. Niiler, Scripps Institution of Oceanography.

- Graham, N. E., 1994: Decadal-scale climate variability in the 1970s and 1980s: Observations and model results. *Climate Dyn.*, **10**, 135–162.
- Hahn, C. J., S. G. Warren, and J. London, 1995: The effect of moonlight on observation of cloud cover at night, and application to cloud climatology. *J. Climate*, **8**, 1429–1446.
- , —, and —, 1996: Edited synoptic cloud reports from ships and land stations over the globe, 1982–1991. CDIA Rep. NDP026B, 45 pp. [Available from Carbon Dioxide Information Analysis Center, Oak Ridge National Laboratory, P.O. Box 2008, Oak Ridge, TN 37831-60500.]
- Harrison, E. F., P. Minnis, B. R. Barkstrom, V. Ramanathan, R. D. Cess, and G. G. Gibson, 1990: Seasonal variation of cloud radiative forcing derived from the Earth Radiation Budget Experiment. *J. Geophys. Res.*, **95**, 18 687–18 703.
- Hasselmann, K., 1976: Stochastic climate models, I. Theory. *Tellus*, **28**, 473–485.
- Klein, S. A., and D. L. Hartmann, 1993: The seasonal cycle of low stratiform clouds. *J. Climate*, **6**, 1587–1606.
- , —, and J. R. Norris, 1995: On the relationships among low-cloud structure, sea surface temperature, and atmospheric circulation in the summertime northeast Pacific. *J. Climate*, **8**, 1140–1155.
- Lindzen, R. S., and S. Nigam, 1987: On the role of sea surface temperature gradients in forcing low-level winds and convergence in the tropics. *J. Atmos. Sci.*, **44**, 2418–2436.
- Mantua, J. N., S. R. Hare, Y. Zhang, J. M. Wallace, and R. C. Francis, 1997: A Pacific interdecadal climate oscillation with impacts on salmon production. *Bull. Amer. Meteor. Soc.*, **78**, 1069–1079.
- Minobe, S., 1997: A 50–70 year climatic oscillation over the North Pacific and North America. *Geophys. Res. Lett.*, **24**, 683–686.
- Nitta, T., and S. Yamada, 1989: Recent warming of tropical sea surface temperature and its relationship to the Northern Hemisphere circulation. *J. Meteor. Soc. Japan*, **67**, 375–383.
- Norris, J. R., and C. B. Leovy, 1994: Interannual variability in stratiform cloudiness and sea surface temperature. *J. Climate*, **7**, 1915–1925.
- Rozendaal, M. A., C. B. Leovy, and S. A. Klein, 1995: An observational study of diurnal variations of marine stratiform cloud. *J. Climate*, **8**, 1795–1809.
- Trenberth, K. E., 1990: Recent observed interdecadal climate changes in the Northern Hemisphere. *Bull. Amer. Meteor. Soc.*, **71**, 988–993.
- , and J. W. Hurrell, 1994: Decadal atmospheric–ocean variations in the Pacific. *Climate Dyn.*, **9**, 303–309.
- Warren, S. G., C. J. Hahn, J. London, R. M. Chervin, and R. L. Jenne, 1988: Global distribution of total cloud cover and cloud type amounts over the ocean. NCAR Tech. Note NCAR/TN-317+STR, National Center for Atmospheric Research, Boulder, CO, 42 pp. + 170 maps. [Available from NCAR, P.O. Box 3000, Boulder, CO 80307.]
- Zhang, Y., 1996: An observational study of atmosphere–ocean interactions in the northern oceans on interannual and interdecadal time scales. Ph.D. thesis, University of Washington, Seattle, WA, 162 pp. [Available from Natural Sciences Library, University of Washington, Seattle, WA 98195.]
- , J. M. Wallace, and D. S. Battisti, 1997: ENSO-like interdecadal variability: 1900–93. *J. Climate*, **10**, 1004–1020.
- , J. R. Norris, and J. M. Wallace, 1998: Seasonality of large scale atmosphere–ocean interaction over the North Pacific. *J. Climate*, **11**, 2473–2481.